Signal-to-noise ratio evaluation in resonant ring metamaterial lenses for MRI applications

2011 New J. Phys. 13 115006

(http://iopscience.iop.org/1367-2630/13/11/115006)

New Journal of Physics
The open-access journal for physics

Signal-to-noise ratio evaluation in resonant ring metamaterial lenses for MRI applications

J M Algarin[1], M A Lopez, M J Freire and R Marques
Department of Electronics and Electromagnetism, Faculty of Physics, University of Seville, Avda. Reina Mercedes s/n, 41012 Sevilla, Spain
E-mail: jalgarin@us.es

New Journal of Physics **13** (2011) 115006 (12pp)
Received 30 June 2011
Published 8 November 2011
Online at http://www.njp.org/
doi:10.1088/1367-2630/13/11/115006

Abstract. In this paper, we present a method for the evaluation of the signal-to-noise ratio in magnetic resonance imaging (MRI) coils loaded with resonant ring metamaterial lenses, in the presence of a conducting phantom resembling human tissue. The method accounts for the effects of the discrete and finite structure of the metamaterial. Numerical computations are validated with experimental results, including laboratory measurements and MRI experiments.

Contents

1. Introduction

Metamaterials are artificial structures that can be tailored in order to achieve a wide range of electromagnetic properties that cannot be observed in nature, including simultaneously negative

[1] Author to whom any correspondence should be addressed.

effective permittivity and permeability [1]. It is well known that a metamaterial slab with relative permittivity ε_r and relative permeability μ_r, both equal to -1, behaves as a 'super-lens' with a resolution [2] well beyond the diffraction limit of classical optics or sub-wavelength (sub-λ) resolution. If the frequency of operation is sufficiently low, we are in the realm of quasi-statics, and we only need a metamaterial slab with $\varepsilon_r = -1$ or $\mu_r = -1$ (depending on the electric or magnetic nature of the quasi-static field) in order to observe this effect [2]. The same effect can be observed in two coupled magneto-inductive (MI) surfaces [3–5]. Effective electromagnetic properties of metamaterials arise from their structure rather than from the nature of their components, which often are conventional conductors and dielectrics. Many metamaterials are made of the periodic repetition of some resonant elements with a sub-λ period, so that some kind of homogenization can be made [6]. Due to the resonant nature of its constitutive elements, the interesting properties of such metamaterials usually appear in a very narrow band of frequencies. This narrow bandwidth is commonly considered as a major drawback for many applications. However, it is not an important limitation for magnetic resonance imaging (MRI), because MR images are acquired by measuring radio-frequency (RF) signals inside a relatively narrow bandwidth of a few tens of kilohertz. Besides, due to the low frequency of operation of most MRI systems (tens of MHz), designing metamaterials with a sub-λ period is an affordable task. Thus, MRI appears as a natural application for resonant ring metamaterials.

As is well known, the generation of images in MRI is based on the detection of spatial variations in the phase and frequency of the RF waves absorbed and emitted by the nuclear spins of the imaged object. MRI detectors are conventional coils operating in the near-field region of the RF magnetic field. Metamaterials offer the possibility of manipulating this magnetic near-field in order to improve coil performance. The application of metamaterials in MRI has been previously explored in several works making use of devices based on different types of resonant elements, such as swiss-rolls [7–11], wires [12] and capacitively loaded split rings [13–16]. Many of these works have explored the sub-λ imaging ability of metamaterials with $\mu_r < 0$. A capacitively loaded split ring is a small open ring of copper that is loaded in the gap with a chip capacitor. Diamagnetic properties of closed inductive loops were well known in the past and Schelkunoff reported that this effect can be enhanced by adding a chip capacitor [17] to the ring. Of course, this capacitor has to be non-magnetic for MRI applications. In previous works, some of the present authors have analyzed the MRI applications of capacitively loaded split-ring metamaterial slabs with effective permeability $\mu_r = -1$. The ability of such metamaterials to increase the sensitivity of surface coils [13, 14] and to improve the localization of the field of view (FOV) of these coils [15] (a fact that may find applications in parallel MRI (pMRI)) were analyzed. pMRI works by taking advantage of the spatially sensitive information inherent in a receiving array of multiple surface coils in order to partially replace time-consuming spatial encoding and thus to reduce the image acquisition time [19, 20]. Moreover, we have also investigated the application of resonant ring slabs with effective permeability $\mu_r \to 0$ to locally increase the signal-to-noise ratio (SNR) of surface coils [16]. Increasing the SNR of the image is one of the main goals in conventional MRI, besides the reduction of the acquisition time.

In a previous work [14], some of the present authors presented a method for the evaluation of the SNR of surface coils in the presence of metamaterial slabs of negative effective permeability. This method was a first approach to the problem, since metamaterial slabs were modeled as continuous slabs with an effective permeability extracted from a previously reported homogenization procedure [18]. Therefore, this model did not take into account the effects of the discrete and finite structure of the metamaterial. Moreover, other metamaterial structures, such as the MI lens reported by the authors [3–5], cannot be modeled by this approach. More recently, a new approach was developed by some of the present authors in order to overcome these drawbacks [21, 22]. This approach, however, was developed for metamaterials operating in vacuum. Therefore, it cannot take into account the effect of human tissues, which is essential for the evaluation of noise. Thus, it would be desirable to include in the analysis the presence of conducting samples resembling human tissues. Such an analysis is developed in this paper, which is organized as follows: in the next section, a method for the computation of the SNR is developed. Next, the experimental validation of the predictions of such a method is presented, and a comparison with the results from the continuous medium approach [14] is made. Then, an example of the application of the proposed method to the optimal design of a metamaterial MRI lens is presented. Finally, some conclusions are presented.

2. Computation of the signal-to-noise ratio

This section shows the details of the method developed for the computation of the SNR of MRI receiving coils in the presence of realistic split-ring metamaterial slabs and conducting samples resembling human tissues. For the sake of simplicity, the sample will be modeled as a conducting half-space, with a conductivity value typical of human tissue. The analysis is divided into two parts corresponding to the signal and the noise. According to reciprocity theorem, the signal received by a coil from a magnetic dipole placed at certain point inside a sample is proportional to the magnetic field per unit current (noted as B_1 in the specialized literature) produced by the coil at that point [23]. On the other hand, the MR noise is proportional to the square root of the noise resistance R associated with the sample [24]. In our analysis, the coil is assumed to be lossless, which means that both the coil losses and MRI system losses are excluded from the analysis. Therefore, the computed noise will be a sort of intrinsic noise [25], associated only with the presence of human tissues and metamaterial. Since we are interested in comparison of the SNR given by different configurations and since the SNR is proportional to $B_1/\sqrt{R}$, in our analysis we will compute and compare this quantity for different configurations. Figure 1(a) shows a sketch of the configuration under analysis: a coil is placed at a distance s from the surface of a split-ring slab of thickness d, which is placed on the interface of a conducting half-space. The goal is to evaluate the SNR at a point located at a distance z inside the sample.

For the analysis, the configuration shown in figure 1(a) is divided into two subsystems. The first subsystem, or subsystem A, consists of the coil and the metamaterial slab as if they were placed in vacuum. The second subsystem, or subsystem B, consists of only the conducting half-space. In general, the metamaterial slab consists of a number N of rings which are periodically arranged in a 3D lattice (see figure 1(b), as an example). In subsystem A, the field produced by the coil at the exit of the metamaterial, as well as the resistance introduced by the lens, R_{lens}, is calculated. This computation is made by following the method reported by us in [21], where the matrix equation for the unknown currents in the rings and coil has been solved. It may be worth noting that analysis of such a structure, with thousands of elements, cannot be performed by means of the available commercial electromagnetic solvers based on standard numerical methods. The matrix equation that has to be solved is $\overline{\overline{Z}} \cdot \overline{I} = \overline{V}$, where $\overline{\overline{Z}}$ is the impedance matrix of the system with $(N+1) \times (N+1)$ elements, which include the N rings of the metamaterial and the coil, $\overline{I}$ is the vector of unknown currents and $\overline{V}$ is the voltage vector, which is set equal to 1 for the coil and to zero for the rings. The diagonal elements

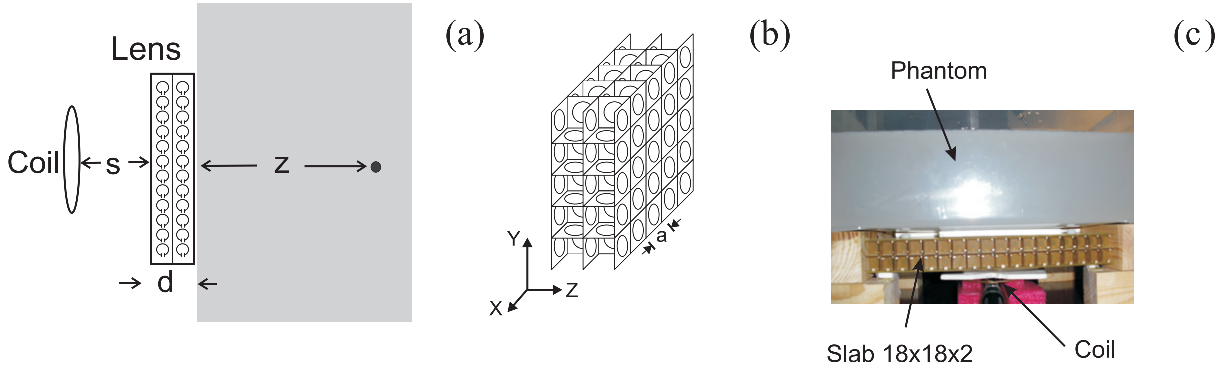

Figure 1. (a) Sketch of the configuration under analysis: a coil is placed at a distance s from the surface of a split-ring slab of thickness d, which is placed at the interface of a conducting half-space. (b) Sketch of the three-dimensional (3D) lattice of rings that constitute the split-ring slab. (c) Photograph of the experimental setup.

$Z_{ii} = R + j\omega L + 1/j\omega C$ correspond to the self-impedances of the rings and coil, where ω is the frequency, R the resistance, L the self-inductance and C the capacitance (in the case of the coil, R and C are taken to be equal to zero). All these parameters can be measured independently, and are treated as external inputs. The non-diagonal elements $Z_{ij} = j\omega M_{ij}$ depend on the mutual inductances M_{ij} between the rings of the metamaterial and between the coil and rings of the metamaterial. The mutual inductances between the rings of the metamaterial are computed using the Neumann formula, which has been tested to provide enough accuracy for our purposes. For the coil, a model based on two filaments [26] was used to account for wide strips. The mutual inductances between the coil and rings of the metamaterial are calculated using this model and the Neumann formula [26]. Symmetries are taken into account in order to reduce the computation time. Once the matrix system is solved and all the currents are obtained, the resistance introduced by the lens, R_{lens}, is given by the real part of the ratio between the imposed voltage in the coil (1 V) and the computed current in this element I_{N+1}: $R_{\text{lens}} = \text{Re}(1/I_{N+1})$. Finally, the vector potential $\vec{A}(x, y, 0)$ at the exit of the metamaterial is computed as the sum $\vec{A}(x, y, 0) = \sum_{i=1}^{N+1} \vec{A}_i(x, y, 0)$, where each summand is computed using standard electromagnetic formulae.

In our analysis, the field at the exit of the metamaterial slab in vacuum in subsystem A is assumed to be the impinging field existing at the input interface of the conducting half-space in subsystem B. This assumption implies that the mutual inductances between the rings calculated in vacuum in subsystem A should be the same in the presence of the conducting half-space. In order to validate this assumption, table 1 shows the mutual inductances obtained for a pair of rings in axial and coplanar configurations, both in vacuum and in the presence of a conducting sample. The dimensions of the rings correspond to the structure of the metamaterial lens previously reported by us [13]. The same structure will be used in the next section for the validation of the predictions of the method. The calculations of mutual inductances shown in the table were obtained with a rigorous full-wave electromagnetic analysis using the commercial electromagnetic solver CST *Microwave Studio*, which can be used for the analysis of the present case with only two rings but not for the whole structure of thousands of rings, as has been mentioned above. In the simulation, the conducting sample ($\sigma = 1.6\,\text{S m}^{-1}$) was finite but large

Table 1. Mutual inductances between two rings, each of external radius 6.02 mm and width 2.17 mm and with their centers separated by 15 mm, in vacuum (M_v) and in the presence of a conducting sample (M_c) for both coplanar and coaxial configurations. The conducting sample ($\sigma = 1.6\,\mathrm{S\,m^{-1}}$) was placed at 1.5 mm distance from the rings.

Case	M_v (nH)	M_c (nH)
Coplanar	−0.170	$-0.170 - j7.49 \times 10^{-3}$
Coaxial	0.216	$0.216 - j4.53 \times 10^{-3}$

enough to avoid edge effects. The results in the table show that the real parts of the mutual inductances obtained in vacuum and in the presence of the conducting sample are quite similar and that the small imaginary part that appears in the presence of the conducting sample can be neglected. Therefore, the main assumption of the present method is valid.

After the analysis in subsystem B, next the vector potential obtained at the exit of the metamaterial in vacuum is decomposed into its spatial Fourier harmonics $\tilde{\vec{A}}(k_x, k_y, 0)$ by means of a fast-Fourier transform (FFT). Next, each harmonic is multiplied by a transmission coefficient, $T(k_x, k_y)$, which accounts for the boundary conditions at the interface between vacuum and the conducting half-space, so that the transmitted harmonics that propagate inside the conducting half-space are given by

$$\tilde{\vec{A}}(k_x, k_y, z) = T(k_x, k_y)\tilde{\vec{A}}(k_x, k_y, 0)\,\mathrm{e}^{-jk_z z}, \tag{1}$$

where $k_z = \sqrt{\omega^2\mu_0\varepsilon - k_x^2 - k_y^2}$ and ε is a complex quantity accounting for the permittivity and conductivity of the half-space, which resembles human tissue ($\mathrm{Re}(\varepsilon) \simeq 90\varepsilon_0$, $\mathrm{Im}(\varepsilon) \simeq -\sigma/\omega$). Once the vector potential is known inside the conducting half-space, the Fourier transform of the magnetic field $\tilde{B}_z(k_x, k_y, z)$ is calculated from the transverse components of the vector potential as

$$\tilde{B}_z(k_x, k_y, z) = jk_y\tilde{A}_x(k_x, k_y, z) - jk_x\tilde{A}_y(k_x, k_y, z). \tag{2}$$

Finally, the magnetic field $\vec{B}_z(x, y, z)$ is obtained by means of an inverse FFT, which provides the signal for the calculation of the SNR.

The conducting half-space introduces in the coil an additional series resistance, R_{cond}, that, from the point of view of the reciprocity theorem, is due to the power dissipated by the eddy currents in the conducting half-space:

$$R_{\mathrm{cond}} = \frac{\sigma}{|I_{N+1}|^2}\int |\vec{E}(x, y, z)|^2\,\mathrm{d}\tau = \frac{\sigma\omega^2}{|I_{N+1}|^2}\int |\vec{A}(x, y, z)|^2\,\mathrm{d}\tau. \tag{3}$$

Taking into account the Parseval theorem, the above expression remains as follows:

$$R_{\mathrm{cond}} = \frac{\sigma\omega^2}{|I_{N+1}|^2}\int_{-\infty}^{+\infty}\mathrm{d}k_x\int_{-\infty}^{+\infty}\mathrm{d}k_y\int_{0}^{+\infty}\mathrm{d}z|\tilde{\vec{A}}(k_x, k_y, z)|^2. \tag{4}$$

Therefore, $\tilde{\vec{A}}(k_x, k_y, z)$ provides both the signal (2) and the additional noise (4) introduced by the conducting sample. With this procedure, both the magnetic field $B_z(x, y, z)$ inside the conducting half-space and the total resistance in the coil $R_{\mathrm{lens}} + R_{\mathrm{cond}}$ can be calculated to finally

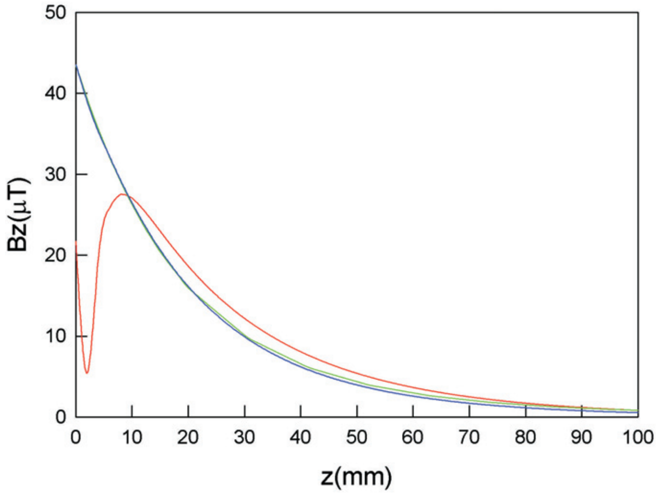

Figure 2. Axial field along the z-direction inside the conducting half-space. The field is produced by a circular coil of 3 inches diameter placed at 15 mm distance from a split-ring slab of thickness 3 cm and $18 \times 18 \times 2$ unit cells with periodicity 15 mm. The slab is separated by 4 mm from the input interface of the conducting slab with conductivity $\sigma = 1.6\,\mathrm{S\,m^{-1}}$. Red: the discrete method; green: the continuous approach; blue: CST simulation.

obtain the SNR as

$$\mathrm{SNR}(x, y, z) = \frac{|B_z(x, y, z)/I_{N+1}|}{\sqrt{R_{\mathrm{lens}} + R_{\mathrm{cond}}}}. \tag{5}$$

All the integrations in the method were numerically obtained by using Romberg's method.

3. Discussion

3.1. Validation of the method

In the above section, we have shown a method for the computation of the SNR that takes into account the effects of the discrete and finite structure of realistic resonant ring metamaterials. In the present section, the predictions of this method, which will be termed the discrete method, are compared with the predictions of the continuous medium approach reported by us in [14] and with the experimental results for a real structure. The real configuration under analysis is similar to that sketched in figure 1(a), and a photograph is shown in figure 1(c). It consists of a circular coil of 3 inches diameter and strip width 1 cm that is placed at 15 mm distance from the metamaterial lens reported by some of the present authors in [13], with this lens placed at 4 mm distance from the input interface of a conducting sample. The sample consists of a $14 \times 16 \times 16\,\mathrm{cm}^3$ phantom filled with a water saline solution with conductivity $\sigma = 1.6\,\mathrm{S\,m^{-1}}$. The lens consists of a 3D array of $27 \times 27 \times 3\,\mathrm{cm}^3$ containing $18 \times 18 \times 2$ cubic cells with a periodicity of 15 mm and a total number of capacitively loaded split rings of 2196 [13]. Each ring contains a non-magnetic capacitor of the series ATC100B specially designed by American Technical Ceramics Corp. (New York, USA) for MRI applications and manufactured with low tolerance for our application. The rings were photoetched on an FR4 substrate. The red line in figure 2 shows the calculation by the discrete method of the axial field $B_z(0, 0, z)$ inside the

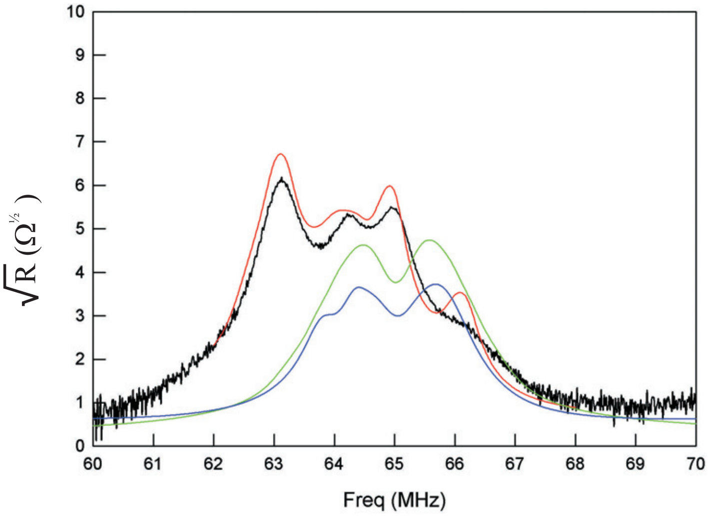

Figure 3. Square root of the input resistance in the coil of the configuration analyzed in figure 2. Red: the discrete method; green: the continuous approach; blue: the CST simulation; black: the measurements with the real split-ring slab and a $14 \times 16 \times 16\,\mathrm{cm}^3$ phantom filled with a water saline solution with conductivity $\sigma = 1.6\,\mathrm{S\,m}^{-1}$.

conducting half-space ($\sigma = 1.6\,\mathrm{S\,m}^{-1}$) which simulates the phantom. The computation has been carried out at a frequency of 63.6 MHz, which corresponds to the Larmor frequency of the MRI scanner used for the experiments. The green line in figure 2 shows the calculation given by the continuous medium approach [14] by modeling the lens as an infinite continuous slab with the same thickness (3 cm) along the z-direction as the real structure and the phantom as a conducting half-space. In this approach, the permeability of this slab is modeled following equation (13) in [18]. Finally, the blue line in figure 2 shows the field given by the electromagnetic solver CST *Microwave Studio* when both the lens and the phantom are modelled with the same parameters as those in the continuous medium approach but with finite dimensions of the real structure.

The comparison of the green and blue curves in figure 2 shows that the continuous medium approach provides the same results on the field for both the infinite and finite cases. The results of the discrete method (red line) show a strong discrepancy with the results of the continuous approach (green and blue lines) for distances of the order of unit cell length. The same conclusion was previously reported in [21] for a similar configuration but in vacuum, that is, in the absence of conducting samples. As was explained in [21], at distances smaller than about one lattice constant, the near field of the individual rings dominates, so that at these distances the total field is remarkably different from the field given by the continuous model. This is a consequence of the discrete structure, which cannot be revealed by a homogenized model. Once the magnetic field is computed, the second part of the analysis is calculation of the resistance seen by the coil or the input resistance in the coil. Figure 3 shows the squared root of the input resistance seen by the coil computed with the discrete model (red line), the continuous approach (green line) and CST software (blue line) and finally the measurements (black line) obtained with an Agilent PNA series E8363B Automatic Vector Network Analyzer.

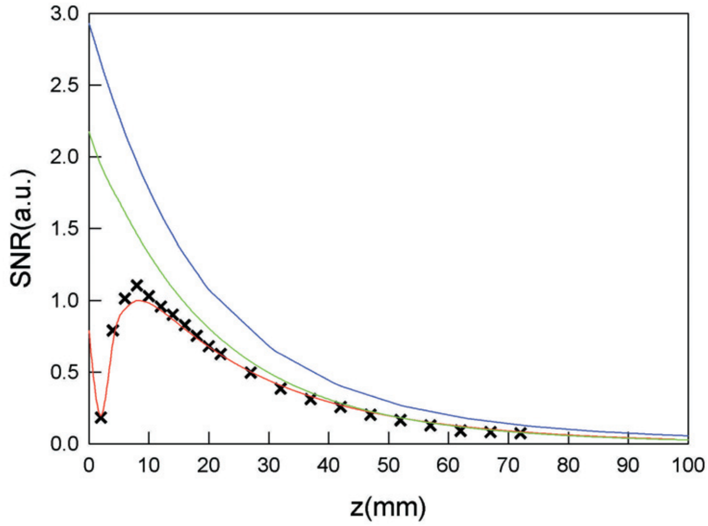

Figure 4. Red: the discrete method; green: the continuous approach; blue: the CST simulation; black: the measurements of the S_{21} coefficient between the coil matched to 50 Ω and a small probe.

Figure 2 shows good agreement between the results given by the discrete method and the measurements in a wide range of frequencies. Next, figure 4 shows the results on the SNR at a frequency of 63.6 MHz. These results correspond to the ratio between the field values shown in figure 2 and the square root of the input resistance shown in figure 3. All the results in figure 4 are normalized to the maximum value obtained with the discrete method (red line) and are shown in arbitrary units. The curve corresponding to the continuous approach for finite size (blue line) is above the curve corresponding to the infinite case (green line). This is due to the fact that the power dissipated by the eddy currents, and therefore the associated input resistance, will always be higher in a semi-infinite sample than in a sample of finite size. The figure also shows the results of the measurement of the SNR (crosses). These measurements correspond to the transmission coefficient (S_{21} parameter in general transmission line theory [28]) measured between the coil matched to 50 Ω (the impedance of the feed) and a small probe placed inside the phantom at different distances z, using the same network analyzer mentioned above. Under these conditions, the S_{21} parameter is proportional to the SNR, as is easily demonstrated in an appendix shown at the end of the paper. This type of measurement is an usual way to characterize the performance of MRI coils in the laboratory previously to the test in the MRI systems. The proportionality constant is obtained by previously fitting both the measured S_{21} and the SNR calculated in the absence of the lens. The coil was matched to 50 Ω by means of a simple matching network consisting of a parallel capacitor and a series capacitor. The figure shows that there is good agreement between the measurements (crosses) and the numerical results given by the discrete method (red line) and that the results provided by the continuous approach disagree both in magnitude and frequency with the measurements.

3.2. Application of the method

Once the method of analysis has been validated, we proceed to use this method for the optimization of an arrangement of split-ring that can provide a good SNR and at the same time

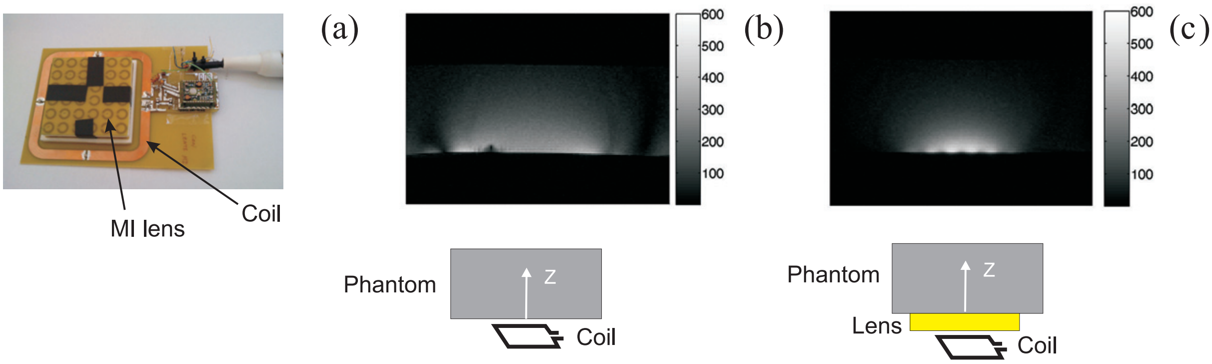

Figure 5. (a) Photograph of a square coil of 12 cm length with an MI lens of 9 cm length placed over it. MR images of a $35 \times 30 \times 10 \times \mathrm{cm}^3$ agar phantom ($\sigma = 0.5\,\mathrm{S\,m^{-1}}$) obtained with (b) the coil and (c) the coil and MI lens.

enhancement of the localization of the FOV of a coil for application in pMRI. The main problem associated with the use of split-ring slabs for pMRI applications is the high noise introduced by the slabs [15]. The result of this optimization process is an arrangement that consists of two parallel arrays of split rings, a structure that was previously studied by us and termed as MI lens [3–5]. The configuration under analysis consists of a squared coil of 12 cm length and 1 cm strip width, and a pair of 2D arrays of $9 \times 9\,\mathrm{cm}^2$, which are parallel to the coil, with 6×6 split rings similar to that of the lens in [13]. The arrays are separated by 11 mm between them and the closest array to the coil is placed at 6 mm distance from it by means of foam layers (see the photograph in figure 5(a)). The coil was actively decoupled by a tuned trap circuit including a PIN diode in transmission. The active decoupling for the loop was −25 dB with and without the metamaterial slab. An MR experiment was carried out using this configuration with a $35 \times 30 \times 10 \times\ \mathrm{cm}^3$ agar phantom with $\sigma = 0.5\,\mathrm{S\,m^{-1}}$. The MR experiment was carried out in a 1.5 T Simphony MR system by Siemens (Siemens Medical Solutions, Erlangen, Germany) at the Virgen Macarena's University Hospital (Seville, Spain). Phantom images with and without the MI lens were acquired using a FLASH sequence (TR/TE: 500/10 ms; FOV $22 \times 22\,\mathrm{cm}^3$; acquisition matrix: 128×128; flip angle: 60°). Figure 5(b) shows an MR image obtained for the agar phantom with the coil. Figure 5(c) shows the image obtained when the MI lens was placed between the coil and the phantom. The images in figure 5 show that the FOV is much better localized laterally with the MI lens.

Next, figure 6 shows the profiles of the SNR measured (black lines) in the phantom along the axis of the coil (z-axis in the sketches shown in figures 5(b) and (c)) in the presence (black solid line) and in the absence (black dashed line) of the MI lens, obtained from a series of phantom measurements [27]. This figure also shows the computation of the SNR for both situations by using the discrete method (red lines) and the measurements of the S_{21} (crosses) in the phantom. The results show that there is good agreement between the simulation and the measurements. The curves show that the SNR provided by the coil in combination with MI lens is the same, for long distances, as that provided by the coil in the absence of MI lens, and that it is even higher for shorter distances when using the lens. This proves that the MI lens can help avoid the main problem associated with the use of metamaterial lenses with surface coils, that is, the high noise introduced by metamaterial slabs [15].

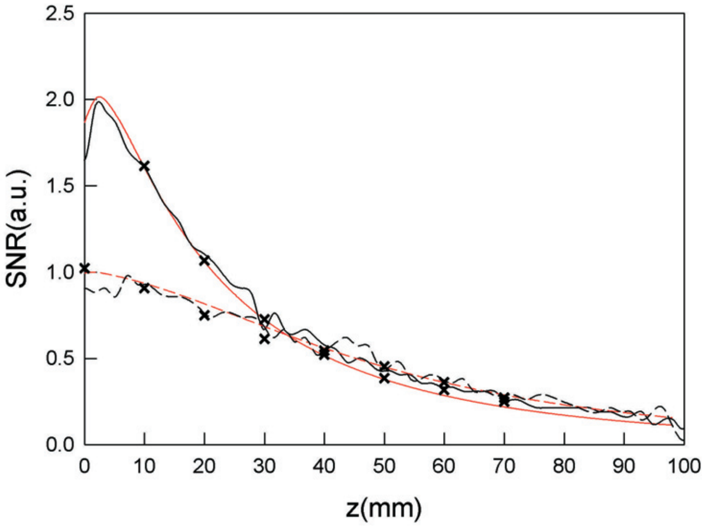

Figure 6. SNR along the z-direction for the configuration of figure 5(b) without the MI lens (dashed lines) and for the configuration of figure 5(c) with the MI lens (solid lines). Red lines: computations provided by the discrete method; black lines: measurements from the MR images; crosses: measurements of the S_{21}.

4. Conclusion

A method has been developed for the computation of the SNR of MRI surface coils in the presence of resonant ring metamaterial slabs and a conducting half-space resembling human tissue. This method accounts for the effects of the discrete and finite structure of realistic metamaterials. Numerical computations provided by this method have been compared with the results provided by a continuous approach and with experimental results, thus making apparent the agreement between the experiment and the predictions of the present method. This method has also been used to optimize a resonant ring metamaterial structure in combination with a surface coil in order to provide good SNR and pMRI capabilities. It has been found that the best option consists of an MI lens slightly smaller than the area of the coil. This configuration has been simulated and the theoretical predictions have been found to agree quite well with the results of an MR experiment.

Acknowledgments

This work was supported by the Spanish Ministerio de Ciencia e Innovacion and European Union FEDER funds under the projects Consolider-EMET CSD2008-00066 and TEC2010-16948 (SEACAM) and by the Spanish Junta de Andalucia under the project TIC-06238 (METAMED). We also thank Dr Carlos Caparros, radiologist from Virgen Macarena's University Hospital in Seville, for his advice.

Appendix A

In this appendix, it is shown how the transmission coefficient, or the S_{21} parameter, between a coil matched to $50\,\Omega$ and a small loop probe is proportional to the SNR provided by the coil. The S_{21} parameter is defined, in general, in the transmission line theory [28] for two-port networks as

$$S_{21} = \left.\frac{V_2^-}{V_1^+}\right|_{V_2^+=0}. \tag{A.1}$$

S_{21} is found by driving port 1 with an incident wave of voltage V_1^+ and measuring the reflected wave amplitude, V_2^-, coming out of port 2; that is, S_{21} is the transmission coefficient from port 1 to port 2 when port 2 is terminated in a matched load ($Z_0 = 50\,\Omega$). The power associated with the wave of voltage V_1^+ is $P = (V_1^+)^2/(2Z_0)$. Since, in our problem, the coil is also matched to $50\,\Omega$ (by means of a simple matching network consisting of a parallel capacitor and a series capacitor), all this power is dissipated in the resistance R which loads the coil; that is, $P = RI^2/2$, where I is the amplitude of the current flowing in the coil and R comes from the losses of the metamaterial and phantom in our experiment. Therefore, V_1^+ can be written as

$$V_1^+ = \sqrt{2Z_0P} = \sqrt{2Z_0}\sqrt{RI^2/2} = I\sqrt{Z_0R}. \tag{A.2}$$

On the other hand, the voltage V_2^- in port 2 is the voltage induced by Faraday's law in the small loop probe, and this voltage can be written as

$$V_2^- = -j\omega B_z S, \tag{A.3}$$

where S is the area of the loop. Substituting the above expressions for V_1^+ and V_2^- into the definition of the S_{21} parameter, we finally obtain

$$S_{21} = V_2^-/V_1^+ = -\frac{j\omega S}{\sqrt{Z_0}}\frac{B_z/I}{\sqrt{R}} = -\frac{j\omega S}{\sqrt{Z_0}}\,\mathrm{SNR}, \tag{A.4}$$

which demonstrates that under the conditions of our experiment (i.e. a coil matched to $50\,\Omega$ and a loop probe of small area) S_{21} is proportional to the SNR.

References

[1] Veselago V G 1968 *Sov. Phys.—Usp.* **10** 509
[2] Pendry J B 2000 *Phys. Rev. Lett.* **85** 3966
[3] Freire M J and Marques R 2005 *Appl. Phys. Lett.* **86** 182505
[4] Freire M J and Marques R 2006 *J. Appl. Phys.* **100** 063105
[5] Freire M J and Marques R 2008 *J. Appl. Phys.* **103** 013115
[6] Marques R, Martin F and Sorolla M 2008 *Metamaterials with Negative Parameters: Theory and Microwave Applications* (Hoboken, NJ: Wiley)
[7] Wiltshire M C K, Pendry J B, Young I R, Larkman D J, Gilderdale D J and Hajnal J V 2001 *Science* **291** 849
[8] Behr V C, Haase A and Jakob P M 2004 *Concepts Magn. Reson.* B **23** 44
[9] Wiltshire M C K 2007 *Phys. Status Solidi* b **244** 1227
[10] Allard M, Wiltshire M C K, Hajnal J V and Henkelman R M 2005 *Proc. Int. Soc. Magn. Reson. Med.* **13** 871
[11] Allard M and Henkelman R M 2006 *J. Magn. Reson.* **182** 200
[12] Radu X, Garray D and Craeye C 2009 *Metamaterials* **3** 90
[13] Freire M J, Marques R and Jelinek L 2008 *Appl. Phys. Lett.* **93** 231108
[14] Freire M J, Jelinek L, Marques R and Lapine M 2010 *J. Magn. Res.* **203** 81
[15] Algarin J M, Freire M J, Lopez M A, Lapine M, Jakob P M, Behr V C and Marques R 2011 *Appl. Phys. Lett.* **98** 014105
[16] Lopez M A, Freire M J, Algarin J M, Behr V C, Jakob P M and Marques R 2011 *Appl. Phys. Lett.* **98** 133508
[17] Schelkunoff S A and Friis H T 1952 *Antennas Theory and Practice* (New York: Wiley) p 584

[18] Baena J D, Jelinek L, Marques R and Silveirinha M G 2008 *Phys. Rev.* A **78** 013842

[19] Griswold M A, Jakob P M, Nittka M, Goldfarb J W and Haase A 2000 *Magn. Res. Med.* **44** 602

[20] Griswold M A, Jakob P M, Heidemann R M, Nittka M, Jellus V, Wang J, Kiefer B and Haase A 2002 *Magn. Res. Med.* **47** 1202

[21] Lapine M, Jelinek L, Marques R and Freire M J 2010 *IET Microw. Antennas Propag.* **4** 1132

[22] Lapine M, Jelinek L, Freire M J and Marques R 2010 *Phys. Rev.* B **82** 165124

[23] Hoult D I and Richards R E 1976 *J. Magn. Reson.* **24** 71

[24] Hoult D I and Lauterbur P C 1979 *J. Magn. Reson.* **34** 425

[25] Edelstein W A, Glover G H, Hardy C J and Redington R W 1986 *Magn. Reson. Med.* **3** 604

[26] Elhawil A, Stiens J, De Tandt C, Ranson W and Vounckx R 2010 *IEEE J. Sel. Top. Quantum Electr.* **16** 380

[27] Ohliger M A, Ledden P, McKenzie C A and Sodickson D K 2004 *Magn. Reson. Med.* **52** 628

[28] Pozar D M 2005 *Microwave Engineering* 3rd edn (Hoboken, NJ: Wiley)